IOP Publishing Measurement Science and Technology
Meas. Sci. Technol. **31** (2020) 045701 (7pp) https://doi.org/10.1088/1361-6501/ab5ea7

10 nm three-dimensional localization using Bessel beam microscopy

Chumki Chakraborty[1], **Md Anisul Islam**[1] **and Craig Snoeyink**[2]

[1] Texas Tech University, Lubbock, TX, United States of America
[2] University at Buffalo, Buffalo, NY, United States of America

E-mail: craigsno@buffalo.edu

Received 4 September 2019, revised 29 November 2019
Accepted for publication 4 December 2019
Published 17 January 2020

Abstract

The last decade has seen significant advances in 3D localization precision driven by demanding applications in biological super-resolution microscopy. These applications have been constrained by precision in the z direction, which had previously been limited to above 10 nm for general applications. Here we present sub-10 nm localization precision using Bessel beam microscopy (BBM) at application-relevant photon counts. BBM uses an axicon, a conical optical element, to transform the point spread function of a microscope to a Bessel pattern, the spatial frequency of which is a simple function of emitter depth. We describe the BBM optical system, outline a method for image analysis, and demonstrate localization of fluorescent silver core silica nanoparticles with better than 10 nm precision in all directions.

Keywords: 3D localization, microscopy, axicon

S Supplementary material for this article is available online

(Some figures may appear in colour only in the online journal)

1. Introduction

The diffraction of light obscures many important cellular and nanoscale physical processes with length scales below roughly 200 nm, also known as the diffraction limit. One method of side-stepping this diffraction limit uses information from the point spread function (PSF) to determine the location of an emitter with precision on the order of nanometers [1]. Techniques enabling localization in three dimensions have been used to shed light on a diverse range of physical systems, from super-resolution microscopy in biology [2] to micro/nanoscale flow characterization [3]. 3D nanoscale localization information has proven crucial to, for example, understanding the dynamics and organization of cell membranes, understanding microtubule networks, understanding flow dynamics inside micro/nanofluidic devices, and many more problems.

These applications have been enabled by a variety of approaches to 3D localization [4–7] with precisions in the range of 20–75 nm in the depth direction, though it is important to note that there is a large variation in reported results due to difficulty in matching experimental conditions (number of photons collected and background noise level). Self-bending [8] (SB-PSF) and interferometric [9] methods have achieved higher precisions compared to others, though SB-PSF is limited by photon loss and interferometric imaging requires a complex optical configuration.

Despite these impressive advancements, many physical phenomena still require localization techniques with precision below 10 nm that are also accessible (i.e. do not require complex optical setups). Here we discuss just such an approach, the 3D localization precision of a microscopy technique called Bessel beam microscopy (BBM), experimentally demonstrating sub-10 nm depth localization precision and sub-5 nm lateral localization precision. In addition, we will also describe an image analysis technique based on maximum likelihood. Using this relatively simple approach, we report localization precisions that, to our knowledge, are significant improvements over the previously reported values.

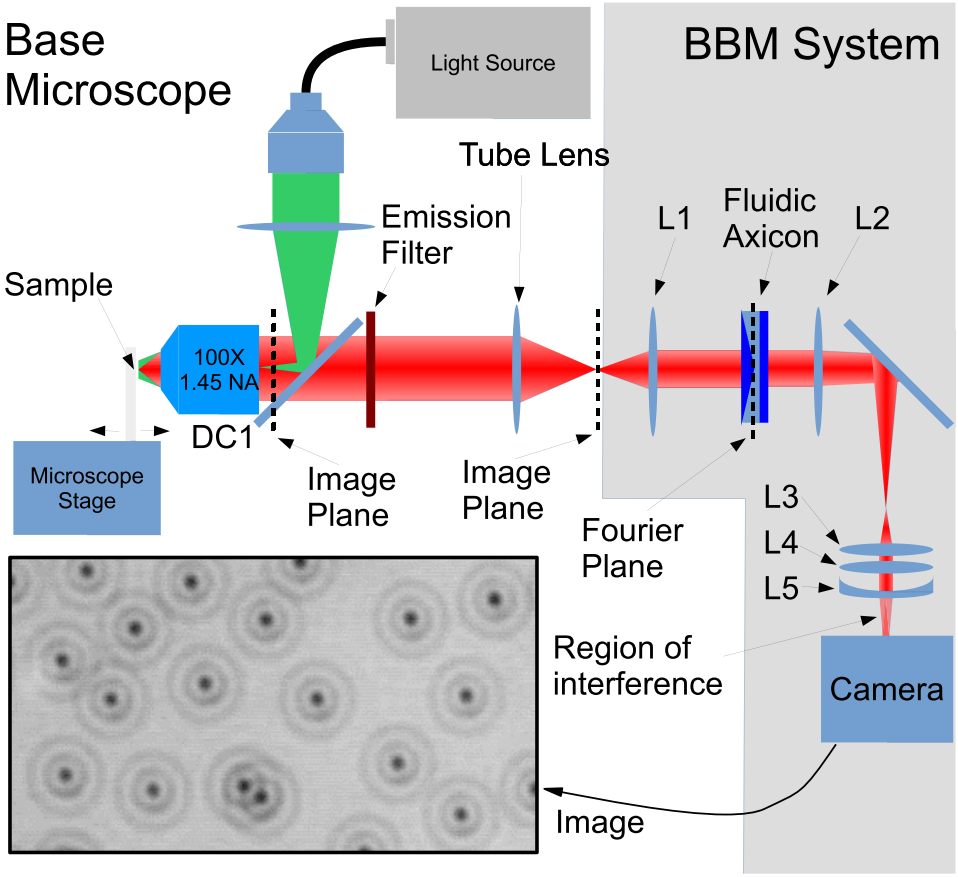

Figure 1. Schematic of the Bessel beam microscopy system and base microscope, with inset example image of fluorescent particles. L1 is a 100 mm achromatic doublet, the fluidic axicon consists of 1° axicon immersed in an index of refraction controlled fluid (aqueous ammonimum thioyanate $n = 1.38$) [10, 11], L2 is a 500 mm plano convex lens, L3 is a 75 mm achromatic doublet, L4 is a 50 mm aspheric lens, and L5 is a −100 mm meniscus CaFl lens. All lenses manufactured by Thor Labs.

2. The principle

Bessel beam microscopy changes the point spread function (PSF) of the microscope to a Bessel pattern, narrowing the PSF and moving energy to concentric side lobes. This Bessel pattern differs from an ideal Bessel beam in its limited extent. As can be seen in figure 1, there are three to four rings around a bright central peak. The mechanism through which the depth information of an emitter is encoded in the Bessel PSF is shown in figure 2. Here, an emitter is shown at three depths relative to the focal plane, as the emitter moves away from the objective the Bessel beam produced by the axicon begins to converge, upscaling the Bessel PSF. When an emitter is farther away than the focal plan the opposite occurs, down-scaling the Bessel interference pattern which occurs in the region of interference.

The optics in a BBM setup, as shown in figure 1, consist of first a lens, L1, immediately after the microscope which aids in making the light beam of an emitter in the focal plane parallel before entering the fluidic axicon by placing it its focal length away from the imaging plane of the microscope. Following the re-imaging lens is an axicon kept in a fluid-filled holder [10] located in the conjugate plane of the microscope objective's back focal plane (Fourier plane). The effective axicon angle is varied by immersing the axicon in aqueous ammonium thiocyanate solutions of various index of refraction [11]. To customize the lateral magnification, localization precision, and sensitivity to depth, an additional system of optics with a different lens combination is placed between the axicon and camera.

This set of optics after the axicon is a Keplerian telescope, well corrected for aberrations. Lenses L2 and L4 form the core of the Keplarian telescope while lens L3 increases the magnification and L5 corrects for aberrations. This optical set serves to improve the Strehl ratio [12, 13], lateral magnification, and depth sensitivity of the system. To aid in the design of BBM systems, the modifying optics can be described using a 2×2 optical system matrix [14] consisting of elements A, B, C, and D. As long as the optics behave as a telescope ($B = 0$), the elements C and D determine the imaging performance for BBM. C gives the lateral magnification for the system, D determines the diameter for the Bessel pattern's central peak and the maximum achievable value of C, both C and D work to determine the depth localization precision of the system. If the modifying optics consists only of free space then $C = L$ and $D = 1$, where L is the distance from the axicon to the camera sensor.

The inset of figure 1 shows the experimentally recorded PSF for a Bessel beam, which can be approximated by

$$I(r) \propto \frac{2kC\alpha^2 (n-1)^2}{w_{ax}^2 D^3} J_0^2(\beta r)\, U\left(\frac{C\alpha (n-1) r}{D w_{ax}}\right)^2 \quad (1)$$

where r is the radius measured from the center of the pattern, J_0 is the zero-order Bessel function of the first kind, k is the wavenumber, α is the effective surface angle of the fluidic axicon, C and D are the respective components of the system matrix representing the optical system described above, n is the index of refraction of the axicon, w_{ax} is the width of the beam incident on the axicon, $U(x)$ is a unit function which is equal to one if $0 \leqslant x < 1$, and β is the spatial frequency of the Bessel pattern [13]. Note that this expression assumes a uniformly intense beam incident upon the axicon. The spatial frequency, β is related to the distance of a point source illuminating the axicon, z_p, through equation (2) [15]. This relationship, described schematically in figure 2 is given by

$$z_p = \frac{\beta C}{\alpha k (n-1) - \beta D}. \quad (2)$$

With the information from the spatial frequency, the apparent distance of the point source can be calculated using this relationship and the lateral location can be determined from the center of the PSF. The relationship between a point source depth and the recorded Bessel PSF is shown in figure 2. When the point source moves towards the microscope objective the beam leaving the objective diverges. This causes the Bessel beam leaving the axicon to diverge, upscaling the Bessel PSF recorded in the image plane. The inverse happens when the particle is farther from the objective than the focal plane. Once the location of the point object is found relative to the axicon, using matrix optics the point source can be translated through the microscope to the measurement volume, determining the location of the particle relative to the objective focal plane and optical axis.

3. Image analysis algorithm

We used a maximum likelihood approach [16] for determining the spatial frequency and center of the Bessel pattern needed for equation (2). The likelihood function which is minimized is

$$f_0 = \min\left(-\sum_{i=1}^{n} \left[d_i \ln\left(g(A, x_c, y_c, \beta, \lambda)\right) - g(A, x_c, y_c, \beta, \lambda)\right]\right) \quad (3)$$

where d_i is the image of the emitter. The function $g(A, x_c, y_c, \beta, \lambda)$ is a simulated Bessel pattern scaled by a photon count A, centered on (x_c, y_c) with a spatial frequency β, with a Poisson-sampled background noise with an expected value of λ, and integrated over a 3×3 sub-sampling of each pixel using Simpson's method [17]. This integration method is computationally efficient and results in an error of less than 0.01% compared to integration of the Bessel PSF using double quadratic integration using the SciPy [18] function *dblquad*.

The function given in equation (3) is non-convex and sensitive to initial guesses and thus prone to convergence to local minima. To encourage optimization to global minima a heuristic has been developed which produces accurate initial guesses. This heuristic starts with a peak search to identify possible particles. A sub-section of the image (window) is taken centered on this point, typically 100×100 pixels, and the background intensity levels of the image are estimated by taking the mode of all pixel values in this window. A smaller window (50×50) is then used to perform the remaining analysis. Next, a radial average is taken about the center of the smaller window to produce a radial intensity profile as shown in figure 3(C) (blue dots). The following function is fit to the radial average:

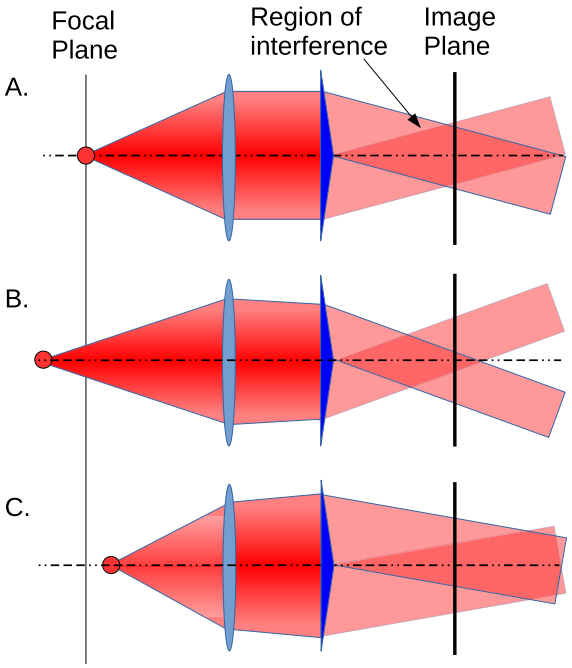

Figure 2. As the point source of light moves towards (C) or away (B) from the microscope objective, the resulting diverging or converging beam of light incident upon the axicon creates a diverging or converging Bessel beam. As a result, the PSF is upscaled or downscaled and the spatial frequency of the recorded Bessel PSF can be directly related to the particle depth (see equation (2)). The Bessel beam occurs in the darker region labeled region of interference and an example of Bessel PSF as imaged in the image plane is shown in figure 1.

$$I(r) = a_1 J_0^2(a_2 r + a_3) + a_4 r + a_5 \quad (4)$$

where r is the distance along the radial average, J_0 is a zero order Bessel function of the first kind, and $a_1 \ldots a_5$ are coefficients to be fitted. The fit is performed using the curve_fit function in the optimization module of SciPy [18] which uses a non-linear least squares algorithm. The a_2 coefficient gives an initial estimate of the spatial frequency of the Bessel pattern.

A linear search is then performed in first the x and then y direction to estimate the location of the emitter relative to the initial guess given by the peak finding algorithm. This search, shown in figures 3(A) and (C), is performed using the estimate of the spatial frequency just found and holding all variables except either x or y constant in equation (3). The minimum value found during the search is used as the best estimate for the x and y coordinates of the center. Finally, the total summed intensity of the Bessel pattern is estimated using a linear

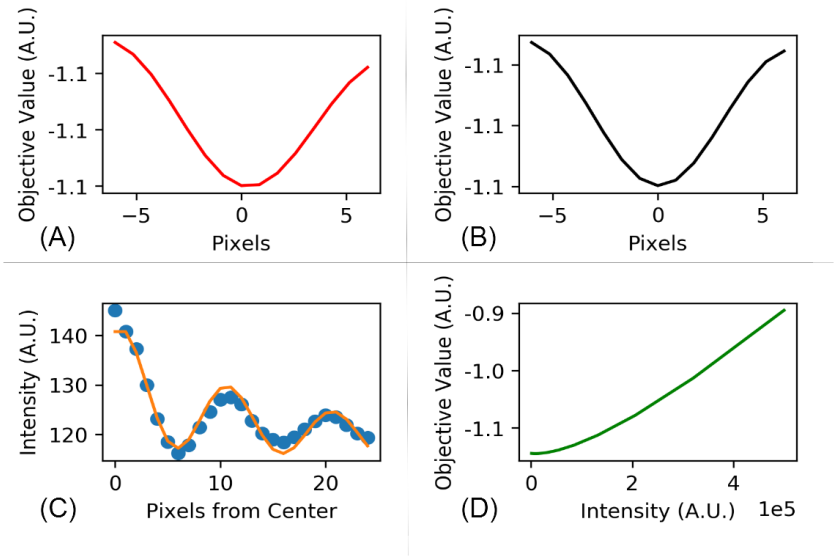

Figure 3. Plots showing heuristics for obtaining high accuracy initial guess. (A) and (B) both show the result of a linear search for the optimal x and y position of emitter, note that the relative change in objective value is small. (C) shows the result of a fit of equation (4) to a radial average of the emitter image. (D) contains the results of a log-linear search in emitter intensity. Note that with the maximum likelihood approach objective values can take arbitrary values but lower is always better.

search with exponentially increasing step sizes as shown in figure 3(C). The current best estimates of the pattern center and frequency are used and held constant and the intensity is increased while looking for the objective minimum, again with equation (3).

The resulting best estimates of background noise, pattern center, spatial frequency, and summed intensity are then used as the initial guess in the fmin_l_bfgs_b function in the optimization module of SciPy [18] which uses the *L-BFGS-B* minimization algorithm [19]. Lastly, the result of the optimization is tested by comparing the final optimized summed intensity value and a second estimate of this value. The second estimate is performed by subtracting the calculated background noise value from the peak intensity value in the window. The estimated total summed intensity that would result in this peak value is then calculated using the final optimized spatial frequency. If the optimized and calculated total summed intensities differ by more than 50% the result is rejected.

4. Experimental methods

For the experiments, we attached the BBM system to a Nikon TI-E microscope with a 100× oil objective (NA 1.49) and an Andor Zyla 5.5 imaging camera. The schematic for the BBM system used for our experiments is shown in figure 1. The light source we used was a Lumencor Spectra X. We used NIS Elements (Nikon) as the imaging software for controlling all these components and for capturing the images.

For the system design, we used a C of 109 mm and D of 0.1 which was achieved through the following lens combination. A 100 mm achromatic doublet was placed 100 mm from the microscope's image plane followed 108 mm along the optical axis by the fluidic axicon [10]. The modifying optics consists of a 500 mm plano convex lens followed 514 mm distance later by a lens cluster of a 75 mm achromatic doublet, 50 mm aspheric lens, and a −100 mm meniscus CaFl lens with spacing of 7 mm and 17.6 mm. The axicon fluid consists of an aqueous ammonium thiocyanate solution with a refractive index of 1.38 [11].

Target particles were Rhodamine 110-dyed fluorescent core shell AgSiO2 nanoparticles synthesized using a sol-gel method [20] for the localization experiments. The Ag core was used for getting higher luminescence due to metal-enhanced fluorescence properties [21]. The particles we synthesized were approximately 90 nm ± 20 nm in size, as demonstrated by dynamic light scattering (DLS), and brighter compared to similarly sized polystyrene counterparts.

The synthesized particles were dried on a glass coverslip and imaged using a 100× oil objective with an NA of 1.49. Epifluorescent illumination was used at 508 nm excitation wavelength and 525 nm emission wavelength. The dried particles were re-immersed in water and stepped through the measurement volume in increments of 50 nm step size taking 100 images at each step. The precision at each step is calculated as the standard deviation of the calculated particle heights. It should be noted that this step size is only slightly larger than the microscope stage step precision, 25 nm, which is denoted by the pink blocks in figure 5. Due to significant stage drift relative to our localization precision, a quadratic is fitted to the set of images at each stage position, and the variation in height is measured from this line, shown as a black line segment in figure 5.

Finally, the number of photons collected per emitter was estimated by comparing to the expected synthetic Bessel patterns. For the synthetic Bessel pattern a fitted function was created that related the peak intensity and number of visible rings to the overall photon count. The peak intensity for an emitter, averaged over the 100 images taken at each step, is then fed into this function to produce the estimated photon count.

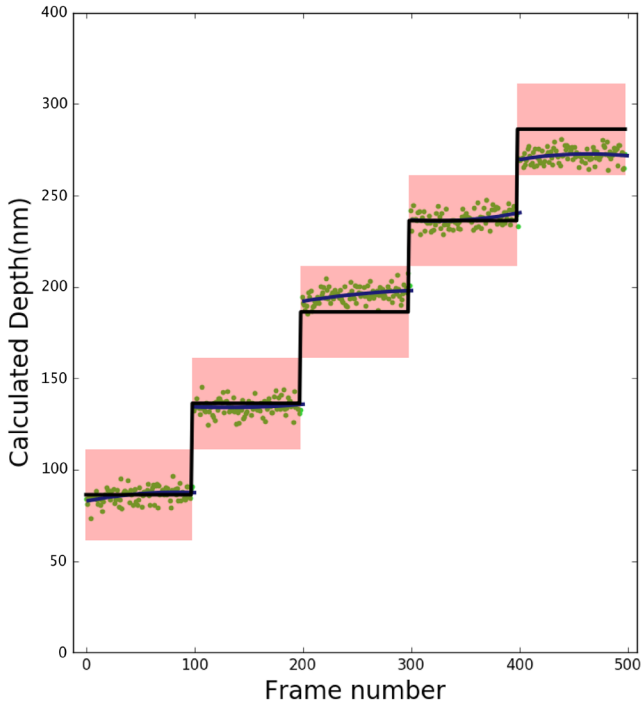

Figure 4. Plot of the calculated depth versus the frame number. The black steps show the movement of the stage, the green scatter shows the z positions of the particle with movement of the stage, and the pink boxes provide a conservative window of 25 nm. The data was fitted with a parabola to take the stage drift into account.

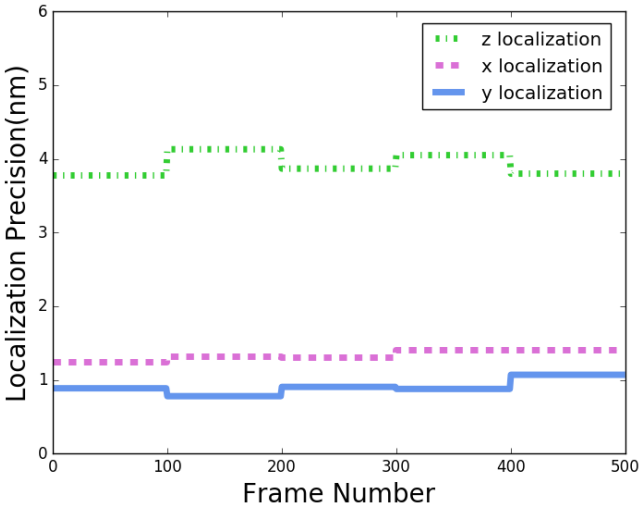

Figure 5. Experimentally calculated localization precision in x, y, and z directions with frame number. Approximately 23 000 photons were collected per frame with a background noise of approximately six photons.

5. Results

An example of data from a precision experiment is plotted in figure 4, where each calculated particle location is plotted as a green dot. Approximately 23 000 photons were collected per frame, with a background noise level of around six photons. At this signal-to-noise ratio, a fairly constant precision of 4 nm in the depth direction and approximately 1 nm in the lateral direction as can be seen in figure 5; in all directions, localization precision was fairly constant with depth. Figure 6 shows a three dimensional scatter plot of the calculated positions of a single particle at a single height. The lack of bias in the estimated particle distributions, as well as the fidelity in reconstructing the stage movements, is remarkable given that no calibration was necessary [15]. Particle images were compared to expected Bessel patterns and, as discussed earlier, once the spatial frequency and image center are known, there is a direct analytical solution to the particle center of luminosity. This latter point, that the algorithm determines the center of luminosity, warrants further discussion.

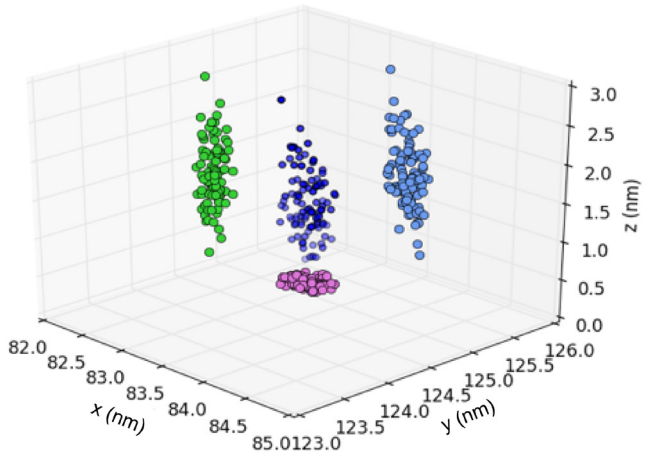

Figure 6. Particle's calculated position from 100 images at a single depth projected in the x (green), y (blue), and z (magenta) showing Gaussian distribution of calculated locations.

When localizing a particle with a precision much smaller than its radius, it is important to distinguish what the algorithm is localizing. The particles imaged here have several tens to hundreds of fluorescent molecules in them. Provided that the particle is small (its image is much smaller than the PSF), the PSF of each emitter will almost entirely overlap. The particles used here, fabricated in house, have imperfections that will affect the distribution of these emitters causing the center of luminosity of the particle to differ from the geometric center of the particle. If this were a physically relevant system this would cause a problem, rolling or tumbling of the particle could cause apparent displacements that are not present. For the experiments in this manuscript the particles were dried and affixed to a glass slide and so were motionless. As a result, the statistical distribution of the localized particle center of luminosity provides a good estimate of the localization precision.

As photon count has a direct implication on the localization precision, we repeated the localization measurements for eight different photon counts, keeping the background photon count approximately constant for all of them.

The localization precision of the BBM system also behaves as expected with respect to photons collected [22]. Figure 7 shows the x, y, and z localization precision at eight different photon counts. Fitting a power law curve to the precision plots results in exponents of between -0.44 and -0.5, very close to the expected dependence of $\approx 1/\sqrt{N}$ as hypothesized in previous literature [1, 22].

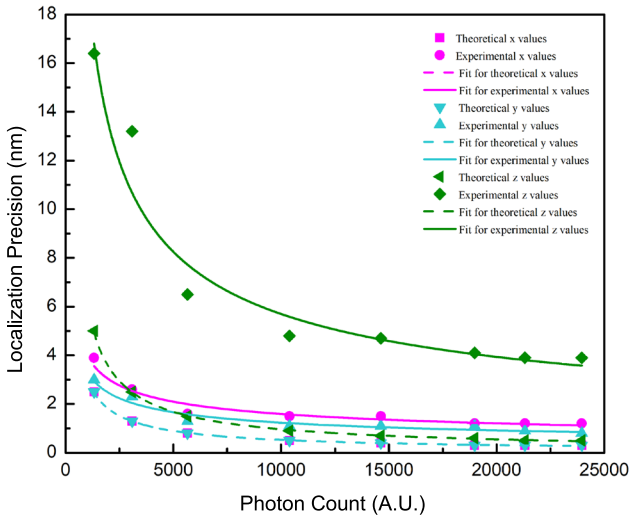

Figure 7. Precision versus photons collected where experimental (solid lines) and theoretical values (dashed) are plotted for x (green), y (blue), and z (magenta).

6. Discussion

There is, however, room to improve the image analysis algorithm. The theoretical precision limit calculated using the Fisher information matrix methodology [22] developed by Ober *et al* is plotted alongside the precision as a function of collected photons in figure 7 as a dashed line. While the lateral precisions are within a factor of 3 of the theoretical precision, the depth precision is more than a factor of 5 higher. It is anticipated that correcting for optical aberrations inherent in high numerical aperture imaging deep within samples will close some of this gap. Additionally, the Bessel pattern images vary from the expected Bessel function, likely due to a variety of imperfections particular to that individual optical setup. These imperfections increase as a function of depth limiting the depth of the measurement volume. Implementing a calibrated image analysis algorithm would take into account these imperfections, likely further improving the precision and increasing the axial range.

This is not the only use of an axicon which can be used to image beyond the diffraction limit of an imaging system. When imaging discrete objects a 40% improvement in diffraction limited resolution has been demonstrated experimentally and this effect has been shown to work synergistically with another super-resolution technique termed structured illumination microscopy [23, 24]. The axicon appears to improve the spatial resolution by altering the angular spectrum of the optical system, essentially applying a frequency shift which increases the maximum frequency while removing the lowest frequencies [23]. This same mechanism could explain the improved localization results shown above.

An alternative way to describe the mechanism of localization precision improvement is to consider how the axicon explicitly encodes phase information in the PSF of the imaging system. As described in figure 2, the axicon produces a Bessel beam which directly encodes the phase information of the emitter beam. The Keplarian telescope added between the axicon and camera magnifies this relationship, enhancing the sensitivity for the system. Further discussion of the relationship between the properties of the axicon, telescope, microscope, and the sensitivity of the system are included in the supplementary material (stacks.iop.org/MST/31/045701/mmedia).

In conclusion, the BBM system is capable of sub-10 nm depth localization precision and sub-5 nm lateral localization precision while collecting less than 5000 photons. This technique requires only fluorescent emitters and that the emitter imaged emitter size is smaller than the PSF. As a result it is suitable for labeled biological samples and fluorescent particle tracking. To the authors' knowledge, this is the lowest reported localization precision reported using a single imaging optical path and off-the-shelf optics. This precision is far from the theoretical limit as estimated using the Fisher information matrix, suggesting that future gains are possible. The authors anticipate that correcting for aberrations common in 3D localization, such as depth-dependent spherical aberration, as well as calibrating the image analysis algorithm, may be a promising area of study in which to realize these gains.

Acknowledgments

Research reported in this publication was supported by the National Institute of General Medical Sciences of the National Institutes of Health under award number R15GM120669. The content is solely the responsibility of the authors and does not necessarily represent the official views of the National Institutes of Health.

This material is based upon work supported by the National Science Foundation under Grant No. 1604398.

ORCID iDs

Craig Snoeyink https://orcid.org/0000-0001-7215-2554

References

[1] Huang B, Bates M and Zhuang X 2009 Super resolution fluorescence microscopy *Ann. Rev. Biochem.* **78** 993–1016
[2] Leung B O and Chou K C 2011 Review of super-resolution fluorescence microscopy for biology *Appl. Spectrosc.* **65** 967–80
[3] Zettner C and Yoda M 2003 Particle velocity field measurements in a near-wall flow using evanescent wave illumination *Exp. Fluids* **34** 115–21
[4] Kao H P and Verkman A S 1994 Tracking of single fluorescent particles in three dimensions: use of cylindrical optics to encode particle position *Biophys. J.* **67** 1291–300
[5] Huang B, Wang W, Bates M and Zhuang X 2008 Three-dimensional super-resolution imaging by stochastic optical reconstruction microscopy *Science* **319** 810–3
[6] Pavani S R P, Thompson M A, Biteen J S, Lord S J, Liu N, Twieg R J, Piestun R and Moerner W E 2009 Three-dimensional, single-molecule fluorescence imaging beyond the diffraction limit by using a double-helix point spread function *Proc. Natl Acad. Sci. USA* **106** 2995–9

[7] Toprak E *et al* 2007 Three dimensional particle tracking by bifocal imaging *Nano Lett.* **7** 2043–5
[8] Jia S, Vaughan J C and Zhuang X 2014 Isotropic three-dimensional super-resolution imaging with a self-bending point spread function *Nat. Photon.* **8** 302–6
[9] Aquino D, Schönle A, Geisler C, Middendorff C V, Wurm C A, Okamura Y, Lang T, Hell S W and Egner A 2011 Two-color nanoscopy of three-dimensional volumes by 4Pi detection of stochastically switched fluorophores *Nat. Methods* **8** 353–9
[10] Akturk S, Arnold C L, Prade B and Mysyrowicz A 2009 Generation of high quality tunable Bessel beams using a liquid-immersion axicon *Opt. Commun.* **282** 3206–9
[11] Borrero-Echeverry D and Morrison B C A 2016 Aqueous ammonium thiocyanate solutions as refractive index-matching fluids with low density and viscosity *Exp. Fluids* **57** 123
[12] Strehl K 1902 Über Luftschlieren und Zonenfehler *Z. Instrum.* **22** 213 (in German)
[13] Snoeyink C 2013 Imaging performance of Bessel beam microscopy *Opt. Lett.* **38** 2550–3
[14] Goodman J W 2017 *Introduction to Fourier Optics* (*Macmillan Learning*) 4th edn (New York: W.H. Freeman)
[15] Snoeyink C and Wereley S 2013 A novel 3D3C particle tracking method suitable for microfluidic flow measurements *Exp. Fluids* **54** 1453
[16] Rieger B and Stallinga S 2014 The lateral and axial localization uncertainty in super-resolution light microscopy *Chemphyschem* A **15** 664–70
[17] Atkinson K E 1989 *An Introduction to Numerical Analysis* (New York: Wiley)
[18] Jones E *et al* 2001 SciPy: open source scientific tools for Python
[19] Byrd R, Lu P, Nocedal J and Zhu C 1995 A limited memory algorithm for bound constrained optimization *SIAM J. Sci. Comput.* **16** 1190–208
[20] Dong M, Tian Y and Pappas D 2015 Synthesis of a red fluorescent dye-conjugated Ag@SiO_2 Nanocomposite for Cell Immunofluorescence *Appl. Spectrosc.* **69** 215–21
[21] Fu Y and Lakowicz J R 2007 Single-molecule studies of enhanced fluorescence on Silver Island films *Plasmonics* **2** 1–4
[22] Chao J, Ward E S and Ober R J 2016 Fisher information theory for parameter estimation in single molecule microscopy: tutorial *J. Opt. Soc. Am.* A **33** B36–57
[23] Snoeyink C and Wereley S 2013 Single-image far-field subdiffraction limit imaging with axicon *Opt. Lett.* **38** 625–7
[24] Perinchery S M, Haridas A, Shinde A, Buchnev O and Murukeshan V M 2019 Breaking diffraction limit of far-field imaging via structured illumination Bessel beam microscope (SIBM) *Opt. Express* **27** 6068–82